ARTICLE

Influencing Solvent Miscibility and Aqueous Stability of Aluminum Nanoparticles through Surface Functionalization with Acrylic Monomers

Christopher A. Crouse,*,†,‡ Christian J. Pierce,† and Jonathan E. Spowart†

Air Force Research Laboratory, Materials and Manufacturing Directorate, Wright-Patterson Air Force Base, Ohio 45433, and UES, Inc., Dayton, Ohio 45432

ABSTRACT With growing interest in the development of new composite systems for a variety of applications that require easily processable materials and adequate structural properties with high energy densities, we have pursued the chemical functionalization of oxide-passivated aluminum nanoparticles (nAl) using three acrylic monomers, 3-methacryloxypropyltrimethoxysilane (MPS), 2-carboxyethyl acrylate (CEA), and phosphonic acid 2-hydroxyethyl methacrylate ester (PAM), to provide chemical compatibility within various solvent and polymeric systems. Fourier transform infrared and X-ray photoelectron spectroscopy suggest that attachment of MPS and PAM monomers occurs through the formation of bonds directly to the passivated oxide surface upon reaction with surface hydroxyls, whereas CEA monomers interact through the formation of ionic carboxylate binding to aluminum atoms within the oxide. The coated particles demonstrate enhanced miscibility in common organic solvents and monomers; MPS and PAM coatings are additionally shown to inhibit oxidation of the aluminum particles when exposed to aqueous environments at room temperature, and PAM coatings are stable at even elevated temperatures.

KEYWORDS: Aluminum • nanoparticles • functionalization • monomer • composites • oxidation

INTRODUCTION

Micrometer-scale aluminum powders (micrometer-Al) are commonly used as additives and/or fuel in various applications requiring high energy output (propulsion, explosives, and pyrotechnics). The increase in specific surface area (SSA) that is gained by replacing micrometer-scale aluminum powders with aluminum nanopowders (nAl) in energetic materials is well documented to have a profound impact on the overall reactivity of the material. Nanopowder formulations are capable of demonstrating reaction rates that are orders of magnitude faster than those observed for conventional formulations prepared with micrometer-sized powders; additionally, these materials also allow for lower ignition times and higher energy output (1−5). This dramatic enhancement in reactivity, because of the high SSA of nAl, has initiated global research efforts focused on replacing micrometer-Al with nAl in modern energetic formulations, in addition to the exploration and development of new formulations based solely upon nAl as the primary fuel (6, 7). Although an increase in SSA is welcomed from the standpoint of material reactivity, it can also be detrimental from the perspective of materials processing and preparation. In general, nanoparticles possess a greater surface energy than larger particles and hence are more susceptible to particle aggregation (to minimize the free energy) (8). Additionally, the high surface area associated with nanopowders can lead to dramatic increases in viscosity when combined with a solvent or polymeric binder during composite preparation and processing (9). Furthermore, as particle size decreases and SSA increases, the relative volume of the passivated oxide layer is no longer negligible and can account for a significant percentage of mass (4). Most commercial nAl powders prepared with a passivated oxide coating typically exhibit 70−85% active (metallic) aluminum content by mass, and the remaining mass is due to the oxide shell on the particles which is an effectively inert material and does not directly participate in the combustion process. Although the passivated oxide layer stabilizes the particles by limiting their pyrophoric nature and providing a protective barrier to further oxidation, under prolonged exposure to air or moisture oxidation can still occur (10). Alternative passivation techniques and/or secondary coatings that are designed to further increase the oxidation resistance of the particles or limit the oxide thickness could potentially expand processing capabilities for these materials (9−14). Additionally, coatings that effectively stabilize the particles under oxidative environments, such as aqueous dispersions, would also be beneficial for applications that utilize water as the primary oxidizing agent.

Chemical functionalization of the nanoparticle surface is a common technique used in the preparation of nanoparticle−polymer composites to minimize particle aggregation

* To whom correspondence should be addressed. E-mail: christopher.crouse@wpafb.af.mil.

Received for review May 7, 2010 and accepted August 1, 2010

† Materials and Manufacturing Directorate.

‡ UES, Inc.

DOI: 10.1021/am100402z

Published on Web 08/26/2010

by altering the chemistry of the nanoparticle surface with an organic corona that is compatible with the polymer. The ligands selected to bridge the gap between the nanoparticle and the polymer matrix are often multifunctional, displaying both a reactive moiety capable of chemically or physically interacting with the nanoparticle surface and an organic component that affords favorable interaction with the polymer matrix (15). The particle architecture for nAl consists of a crystalline metallic aluminum core stabilized by a thin (2−6 nm) amorphous aluminum oxide shell on the exterior of the particle. Altering the surface chemistry therefore requires ligands that are capable of chemically (or physically) interacting with the amorphous aluminum oxide surface. Under standard atmospheric conditions, the amorphous oxide layer can become partially hydroxylated (16), thereby providing a route toward chemical functionalization (17−20). Several groups have explored the formation of self-assembled monolayers (SAMs) on the oxide surface of bulk aluminum and other metal oxide surfaces utilizing the condensation of carboxylic acids to surface-bound hydroxyls (17, 19−21). Successful functionalization of alumina surfaces with silanes (22−24) and phosphoric acids (25, 26) has also been reported. Similar approaches have also been explored and applied to incorporate alumina nanoparticles into polymer composites (27, 28), yet only limited examples exist in which the functionalization of nAl with organic ligands through modification of the thin passivated oxide layer has been investigated. For example, the work of Liu et al. (29, 30) has demonstrated that organosilanes can be used to effectively alter the surface chemistry of flaky aluminum particles to promote dispersion in poly(methyl methacrylate) for pigment applications.

Developing new nAl composite systems that possess adequate structural properties while also maintaining the energetic properties necessary to meet a desired application often requires the use of very large particle loadings; therefore, chemical interaction between the particles and the matrix in which they are imbedded is desired for improving the mechanical properties of the material. To this end, we have pursued the chemical functionalization of commercially available aluminum nanoparticles using three acrylic monomers, 3-methacryloxypropyltrimethoxysilane (MPS), 2-carboxyethyl acrylate (CEA), and phosphonic acid 2-hydroxyethyl methacrylate ester (PAM), to afford compatibility within various polymeric systems. Detailed characterization of these novel coatings along with their impact on the reactivity of the nAl powder is presented.

MATERIALS AND METHODS

Chemicals. Aluminum powder (<50 nm spherical, 18 nm mean particle size, lot C11T058) was purchased from Alfa Aesar and stored under argon in a glovebox (≤1 ppm O_2; dew point of −80 °C) prior to use. 3-Methacryloxypropyltrimethoxysilane (MPS), 2-carboxyethyl acrylate (CEA), phosphoric acid 2-hydroxyethyl methacrylate ester (PAM), methyl methacrylate (MMA), cyclohexanone, 2,2′-azobis(2-methylpropionitrile) (AIBN), and hydroquinone were purchased from Aldrich and used as received unless otherwise noted. Toluene and acetonitrile were obtained from Fisher Scientific and were dried by refluxing over CaH_2 followed by distillation prior to use. MMA and cyclohexanone were also dried over CaH_2 and distilled prior to use. AIBN was recrystallized from acetone prior to use.

Table 1. Reaction Conditions for Monomer Functionalization of nAl

	nAl	monomer (g)			solvent (mL)	
sample	(g)	MPS	CEA	PAM	toluene	acetonitrile
MPS-*co*-nAl	1.0	2.48	−	−	100	−
CEA-*co*-nAl	1.0	−	1.44	−	100	−
PAM-*co*-nAl	1.0	−	−	2.38[a]	−	100

[a] The average molecular weight for PAM was calculated to be 238.14 g/mol based upon a 25% diester content.

Monomer Functionalization of nAl. The specific reagent concentrations used to prepare the monomer-functionalized particles are listed in Table 1. A typical reaction for the functionalization of nAl with CEA to yield CEA-*co*-nAl was performed as follows. A 250 mL, four-neck round bottom flask, fitted with an overhead stirrer, two rubber septa, and a glass stopper, was charged with nAl powder (1.0 g, 37 mmol) and hydroquinone (0.050 g, 0.45 mmol), which was added as a radical scavenger to prevent polymerization during the reaction. A nitrogen atmosphere was established and maintained in the reaction vessel. In a separate 100 mL, single-neck round bottom flask, CEA (1.48 g, 10.0 mmol) was dissolved in 100 mL of dry toluene under nitrogen. The monomer solution was transferred via canula to the reaction vessel, and stirring (250 rpm) was started. The reaction vessel was then submerged in an external oil bath held at 60 °C. The reaction was allowed to progress for 16 h, and samples were removed at specific time intervals to monitor the reaction progress. The functionalized particles were isolated by vacuum filtration over a 0.2 μm PTFE membrane and washed with toluene and acetone to remove the physisorbed monomer. The filtered product was then dried in a vacuum desiccator to remove residual solvent prior to analysis. Surface functionalization of nAl with MPS and PAM monomers to yield MPS-*co*-nAl and PAM-*co*-nAl, respectively, was performed using the same procedure described above with the exception that CH_3CN was used as the solvent for PAM functionalization as noted in Table 1.

Synthesis of Poly(2-carboxyethyl acrylate). A three-neck round bottom flask, fitted with rubber septa and a magnetic stir bar, was charged with CEA (10.0 g, 0.069 mol) and then sealed and placed under a nitrogen atmosphere. AIBN (0.100 g, 0.61 mmol) was dissolved in dry toluene (25 mL) and added to the reaction vessel via the use of a cannula. The vessel was then immersed in an oil bath at 75 °C and held for 2 h with continuous stirring. Upon reaction, the solution increased in viscosity and eventually formed a translucent gel as the polymer precipitated. Heat was removed, and the reaction mixture was allowed to cool. The polymer was isolated by vacuum filtration and washed with acetone to remove the residual monomer and solvent. The final product was dried open to air and then placed into a vacuum desiccator overnight to remove residual solvent. The yield was 9.45 g (94.5%).

Synthesis of Poly(phosphoric acid 2-hydroxyethyl methacrylate ester). A three-neck round bottom flask, fitted with rubber septa and a magnetic stir bar, was charged with PAM (7.0 g, 0.029 mol) and then sealed and placed under a nitrogen atmosphere. AIBN (0.070 g, 0.43 mmol) was dissolved in dry cyclohexanone (25 mL) and added to the reaction vessel via the use of a cannula. The vessel was then immersed in an oil bath at 75 °C and held for 2 h with continuous stirring. Upon reaction, the solution experienced an increase in viscosity and eventually formed a white gel as the polymer precipitated. Heat was removed, and the reaction mixture was allowed to cool. The polymer was isolated by vacuum filtration and transferred

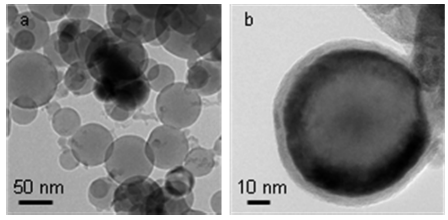

FIGURE 1. TEM images of (a) commercial nAl obtained from Alfa Aesar and (b) a single particle to show the typical particle architecture consisting of an aluminum core and amorphous aluminum oxide passivation layer.

to a Soxhlet extractor where it was washed with acetone for 16 h to remove the residual monomer and solvent. The polymer was then dried open to air and placed into a vacuum desiccator overnight to remove the residual solvent. The yield was 6.44 g (92.0%).

Characterization. Thermogravimetric analysis (TGA) was performed on a TA Instruments SDT Q600 dual TGA/DTA device. Samples (5−20 mg) were placed into a tared alumina crucible with an empty alumina crucible serving as the reference. All data were collected in dynamic mode under flowing argon (100 mL/min) from room temperature to 600 °C at a rate of 10 °C/min.

Fourier transform infrared (FTIR) absorption spectra were obtained from dry powders on a Perkin-Elmer L100 FTIR absorption spectrophotometer equipped with an attenuated total reflectance (ATR) sample attachment.

High-resolution transmission electron microscopy (HR-TEM) images were acquired on a FEI Titan HR-TEM instrument with a CS corrector at an operating voltage of 300 keV. Samples were prepared by drop-drying a dilute solution of functionalized particles suspended in acetone or hexanes onto a 200-mesh copper grid coated with a holey carbon film (Ted Pella, Inc.).

X-ray photoelectron spectroscopy (XPS) was performed on a Surface Science Instruments M-Probe using monochromatic Al K_α X-rays (energy of 1486.6 eV). We prepared XPS samples by casting a drop of functionalized particles suspended in acetone or hexanes onto a 10 mm × 10 mm silicon wafer coated with a native oxide and allowing the solvent to evaporate leaving behind a thin film. CasaXPS was used for curve fitting and interpretation of XPS signals.

RESULTS AND DISCUSSION

The nAl particles used in this study exhibit a core-shell type structure with an amorphous oxide passivation layer (ca. 4 nm) and a crystalline metallic aluminum core (Figure 1). The particle size distribution for the neat material was broad, displaying a mean size of 80 ± 47 nm as determined via TEM analysis. Aggregation and the presence of fused oxide layers between adjacent particles were also observed in the raw material. The active aluminum content of the powder was determined to be 73.6% by measuring the mass gain due to oxidation in the TGA under an 80:20 argon/oxygen mixture. Additionaly, the active aluminum content was stable over the course of this work. The monomeric ligands used in this study, MPS, CEA, and PAM, were selected because of their silane, carboxylic acid, and phosphoric acid moieties, respectively, which are known to react with the surface hydroxyls present on aluminum oxide, thereby covalently anchoring the monomers to the oxide surface (17, 19−26), as illustrated in Scheme 1. Furthermore, the acrylic portion of each ligand should provide the opportunity to directly incorporate the particles into nanocomposite systems.

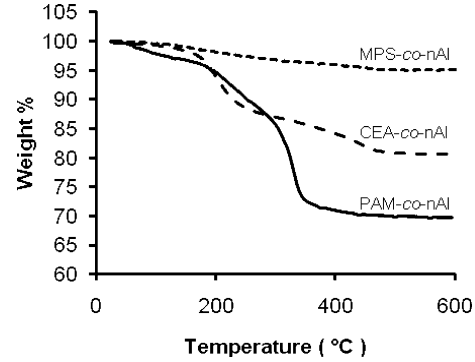

FIGURE 2. Overlay of TGA curves for MPS-*co*-nAl, CEA-*co*-nAl, and PAM-*co*-nAl after 16 h.

Thermogravimetric Analysis (TGA). TGA was used to monitor the reaction efficiency by measuring the mass loss due to the decomposition of the organic component within each powder. The organic should primarily be comprised of monomer, either physisorbed, bound, or in polymer form, on the particle surface. An argon atmosphere was maintained for all TGA analyses to prevent oxidation of metallic aluminum. Figure 2 contains an overlay of the TGA curves acquired for the three monomer-functionalized powders after reaction for 16 h. As a measure of the reaction efficiency, eq 1 was used to calculate an approximate surface density (number of molecules per square nanometer) for each monomeric ligand.

Scheme 1. Illustration Demonstrating Monomer Functionalization of Oxide-Passivated nAl and Chemical Structures for the Described Monomeric Ligands

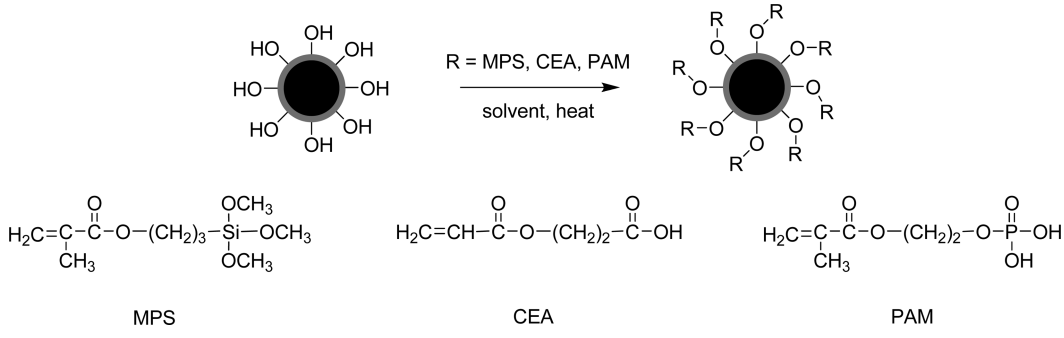

$$\text{grafting density} = \left(\frac{\text{wt \%}}{100 - \text{wt \%}}\right)\frac{6.02 \times 10^{23}}{\text{MW} \times \text{SSA}} \quad (1)$$

where wt % is the weight percentage due to loss of ligand as determined from TGA analysis and MW is the molecular weight for the ligand of interest. SSA for the neat Alfa Aesar nAl particles was estimated to be 33.1×10^{18} nm^2/g based upon particle size distribution data obtained from TEM analysis. This estimated SSA value compares favorably with those of nAl powders available from other manufacturers (31). The grafting densities calculated for the three ligands are listed in Table 2.

Decomposition of MPS-*co*-nAl occurs gradually with no significant loss below 100 °C. The loss between 100−500 °C accounts for ca. 4.5% of the sample weight, with the primary loss occurring above 200 °C. This implies that the organic layer is relatively thermally stable, signifying that MPS is not simply physisorbed but instead interacts with the particle surface likely through the formation of covalent bonds to the oxide. Previous studies that explored the formation of SAMs from alkanesiloxanes on SiO_2/Si surfaces specify a grafting (packing) density equal to 4−5 molecules/nm^2 obtained for the monolayers (32). Because the hydroxyl density on amorphous aluminum oxide is reported to be 3−15 nm^{-2}, approximately 1−3 times greater than that of SiO_2/Si surfaces (33), a monolayer of monomeric ligands employed in our study would experience a density similar to, or slightly greater than, that reported for alkylsiloxanes on SiO_2 if differences between the organic components are assumed to have a negligible impact on packing efficiency. If this assumption is applied, a grafting density of 3.3 molecules/nm^2 would suggest that MPS reacts to form a near monolayer coating on the particle surface after reacting for 16 h.

The decomposition of CEA-*co*-nAl displayed a three-stage loss accounting for ca. 23% of the sample weight. This appreciably larger loss suggests that a large percentage of the ligand on the surface of the particle is physisorbed or has undergone polymerization. The minor loss between 100 and 200 °C is due to evaporation of the physisorbed monomer, while the more significant loss between 200 and 320 °C is believed to correspond to two separate events that occur simultaneously. First, the decomposition of any CEA that was covalently bound to the oxide surface would be expected to occur during this temperature range. Second, if any polymerization did occur during the course of the reaction, then decomposition and depolymerization of the polymer could also occur over this temperature range. Acrylic polymers, when produced by free radical polymerization, undergo decomposition and depolymerization in multiple stages if they contain any unsaturated double bonds at the chain ends or head-to-head bonding present in the polymer backbone (34, 35). Furthermore, because the CEA monomers are terminated with a carboxylic acid on the pendant group, adjacent monomer units could also react through condensation, yielding an anhydride and eliminating water as is observed in the decomposition of poly(acrylic acid) and poly(methacrylic acid) (36, 37). If no polymer or adsorbed monomer were present, then dehydration to form an anhydride would not be possible because the carboxylic acid portion of the monomer would be bound to the oxide surface and not free to react with adjacent monomers.

Table 2. Monomer Grafting Densities Calculated from TGA Mass Loss

sample	$MW_{monomer}$ (g/mol)	mass loss (wt % TGA)	grafting density (no. of molecules/nm^2)
MPS-*co*-nAl	248.35	4.5	3.3
CEA-*co*-nAl	144.13	23	37
PAM-*co*-nAl	238.14[a]	29	31

[a] The average molecular weight for PAM was calculated to be 238.14 g/mol based upon a 25% diester content.

To confirm if polymer was present in the sample, we prepared poly(2-carboxyethylacrylate) from the CEA monomer using AIBN as an initiator. Decomposition of the poly(2-carboxyethyl acrylate) (Figure S1 of the Supporting Information) demonstrates a multistage weight loss curve similar to that observed for CEA-*co*-nAl. The initial loss at 200−300 °C indicates that unsaturated end groups are likely present; condensation of carboxylic acids to form anhydrides could also occur in this temperature range. The second loss, 350−450 °C, occurs due to decomposition and depolymerization from the more stable saturated chain ends. The similarities between decomposition of CEA-*co*-nAl powder and poly(2-carboxyethylacrylate) leads us to believe that CEA exists in the form of both the grafted monomer and polymer on the nAl surface. It is the presence of the polymer that is responsible for the high grafting density that was observed for this ligand.

The mass loss due to decomposition of ligand in PAM-*co*-nAl accounted for ca. 29% of the sample weight. The initial loss, 50−250 °C, is due to the physisorbed (unbound) monomer. This was followed by a second loss, 250−350 °C, attributed to the monomer that is covalently anchored to the oxide surface. Because the calculated grafting density for PAM-*co*-nAl is higher than would be expected for a monolayer coating of the ligand, it is possible, as in the case of CEA-*co*-nAl, that polymerization may have occurred during the course of the reaction. To confirm if the polymer was present in the sample, we prepared poly(phosphoric acid 2-hydroxyethyl methacrylate ester) from the PAM monomer using AIBN as an initiator in the absence of nAl. An overlay comparing the decomposition of PAM-*co*-nAl with both the PAM monomer and poly(phosphoric acid 2-hydroxyethyl methacrylate ester) (Figure S2 of the Supporting Information) indicates that the decomposition of PAM-*co*-nAl is very different from that of poly(phosphoric acid 2-hydroxyethyl methacrylate ester). Therefore, it is unlikely PAM exists in polymer form on the particle surface but could still exist in the form of a strongly adhered multilayer, thus leading to the larger than anticipated surface grafting density.

Following our initial TGA investigation, a time dependence study was performed to monitor reaction progression to determine the time required to achieve complete func-

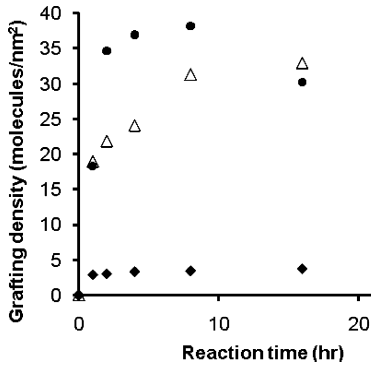

FIGURE 3. Time dependence of functionalization grafting density for (◆) MPS-*co*-nAl, (●) CEA-*co*-nAl, and (△) PAM-*co*-nAl.

tionalization for each monomer. Reactions were performed using the procedure described in Materials and Methods, with sample aliquots being removed from the reaction vessel at specified time intervals of 0.5, 1, 1.5, 2, 4, 8, and 16 h. TGA analysis was again used to determine the mass loss attributed to the respective ligands in each of the functionalized samples. These values were then converted to a grafting density using eq 1 and plotted with respect to the total reaction time (Figure 3).

The data presented in Figure 3 indicates that a maximum grafting density is achieved, irrespective of the monomeric ligand, in less than 8 h at 60 °C. Previous studies that explored the grafting of MPS onto larger, flaky aluminum particles for pigment applications reported that reaction times on the order of 24 h were needed to achieve complete functionalization at room temperature (29). It was also shown that an increase in temperature resulted in more efficient grafting for MPS on flaky aluminum (29), which was the basis for the use of elevated temperatures in our functionalization reactions. Our results, however, demonstrate that much shorter reaction times were necessary to achieve a similar degree of functionalization. This observed increase in the reaction rate for MPS functionalization on nAl is likely attributed to the dramatic increase in the overall SSA associated with the nAl particles. The slightly higher temperatures present under our reaction conditions would also be expected to accelerate the functionalization process. Though the addition of a functionalized layer to the surface of the particle does contribute to the overall mass of the powder and therefore effectively lowers the mass of active aluminum, the ratio of active aluminum to reacted aluminum (aluminum present in the oxide shell) is unaffected by the functionalization process and remains the same as that of the original neat nAl powder.

Surface Analysis. HR-TEM images of the functionalized powders were able to provide visual evidence of the monomer coatings on the oxide surface for all three systems. The images (displayed in Figure 4) show a continuous organic coating present on each of the functionalized powders. Despite functionalization, the TEM images demonstrate that the particles remain aggregated, indicating that functionalization, though effective at altering the chemistry of the particle surface, has little effect on breaking up the large aggregates of particles. Though functionalization is a

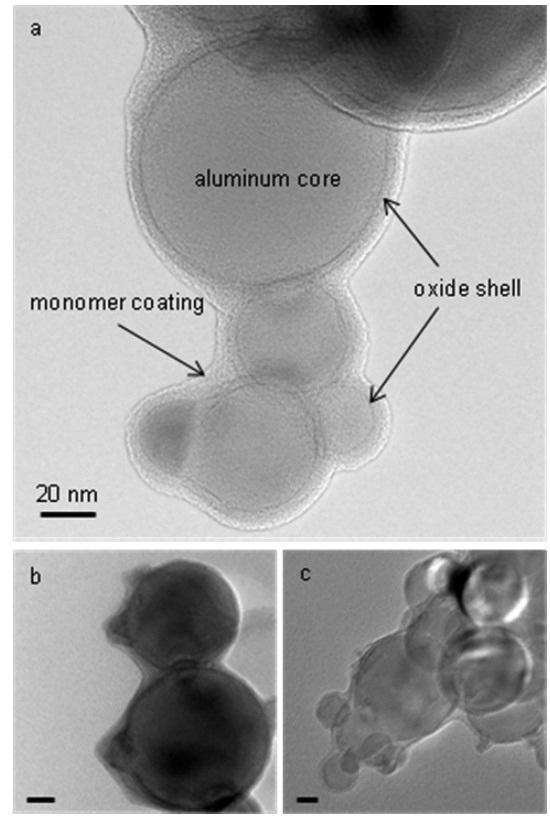

FIGURE 4. TEM images of monomer coatings on nAl: (a) MPS-*co*-nAl, (b) CEA-*co*-nAl, and (c) PAM-*co*-nAl. Scale bars are 20 nm.

technique commonly used to prevent or minimize aggregation in other particle systems, the mild conditions that were utilized in this study, e.g., simple stirring as opposed to high-power sonication or high-shear mixing, would not be expected to break up particles that are strongly adhered to each other. Additionally, this observation can possibly be explained by the presence of fused layer oxides that are formed during the passivation process and result in multiple particles sharing a common oxide layer, thereby permanently linking the particles together.

FTIR analysis of the functionalized powders was performed to confirm the addition of the respective ligands to the nAl surface and to provide insight into their specific bonding interactions. Figure 5 shows FTIR spectra that were obtained for each of the dry functionalized powders and the neat (unfunctionalized) nAl powder. The spectrum for neat nAl was rather featureless aside from the presence of a broad peak at 3305 cm^{-1} that indicates the presence of hydroxyls on the amorphous oxide surface. Additionally, an intense, yet broad, peak that appears at low wavenumbers (900−750 cm^{-1}) confirms the presence of Al−O bonds in the amorphous oxide layer (38). The spectra of the ligand-functionalized nAl powders were clearly different from that of the neat powder, each displaying peaks attributed to their respective monomeric ligand that were not present in the neat nAl powder. A summary of the characteristic peaks and their assignments for each of the functionalized powders and the unfunctionalized nAl are presented in Table 3.

The absorptions observed for MPS-*co*-nAl powder were much less intense than those observed for the other func-

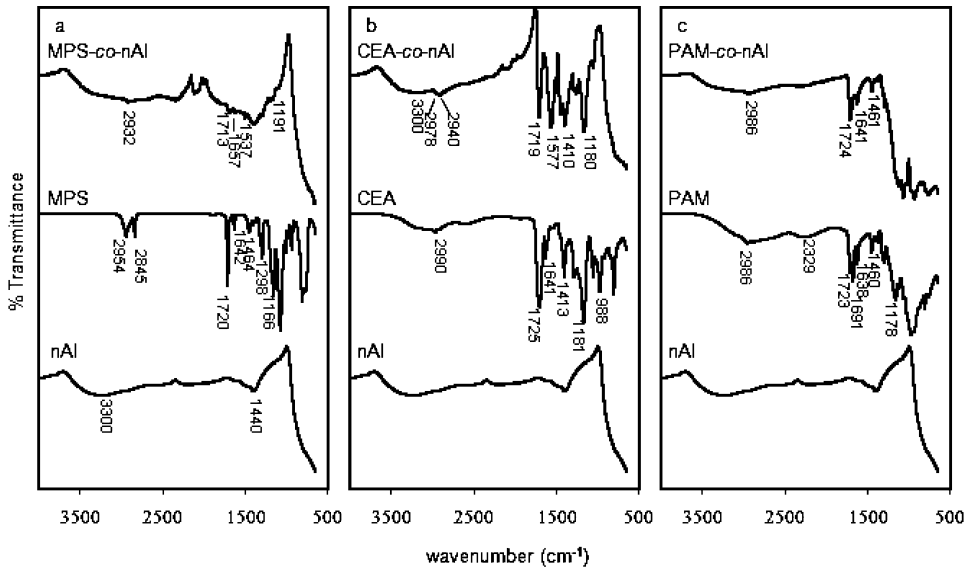

FIGURE 5. Overlays of FTIR spectra recorded for (a) MPS-*co*-nAl, (b) CEA-*co*-nAl, and (c) PAM-*co*-nAl in comparison to those of the respective neat monomers and nAl.

tionalized powders because of the low organic content present on the oxide surface. The presence of weak peaks due to aliphatic C−H stretching, C═O and C−O−C in the methacrylate ester, and C═C confirms the addition of the ligand on the surface. The presence of a broad shoulder centered at 3300 cm^{-1} suggests that some OH groups on the oxide surface remain unreacted. The absence of a strong peak between wavenumbers 1100 and 1000, due to Si−O−Si stretching, suggests it is unlikely that MPS has undergone reaction with itself during the functionalization process to form a significant siloxane network at the particle surface as was observed in previous studies with organosilanes on alumina surfaces (39). This is most likely due to the dry environment utilized in our reactions as these reactions are typically catalyzed by the presence of moisture.

Similar observations were made with the spectrum of CEA-*co*-nAl. Weak peaks arising from aliphatic C−H stretching accompanied by strong peaks due to absorptions from C═O stretching confirm the addition of CEA. The intense peak at 1574 cm^{-1} was assigned to COO^-, suggesting that the majority of the monomer is attached to the oxide surface through an ionic COO^-Al^+ interaction. Other researchers studying octadecanoic acid monolayers on sapphire substrates have attributed this peak to bidentate interactions of the carboxylate with individual aluminum atoms at the oxide surface (19). The lack of an absorption from C═C stretching at 1640 cm^{-1} can possibly be explained by the intensity of the COO^- stretch overlapping with the C═C stretching region. Additionally, the C═C peak would also be absent if polymerization had occurred during the course of the reaction, as was suggested by the TGA data, because the unsaturated C═C would become saturated during polymerization.

The spectrum for PAM-*co*-nAl demonstrates absorptions due to aliphatic C−H stretching as well as C═O and C═C stretching. Additionally, the peak appearing at 954 cm^{-1} suggests that P−O−C stretching is also present. As these absorptions are absent from the neat nAl powder, their presence confirms the attachment of PAM to the oxide surface.

XPS spectra were acquired in parallel with FTIR data collection. Survey spectra (Figure S3 of the Supporting Information), probing binding energies from 0 to 1000 eV (0−600 eV are displayed), were obtained for the neat nAl powder and the three dry functionalized powder samples to confirm their elemental composition. All of the samples, including the unfunctionalized nAl powder, displayed peaks corresponding to O1s (532 eV), C1s (285 eV), Al2p (73 eV), and Al2s (120 eV) peaks. The presence of a C1s signal in the nAl spectra arises from background carbon in the chamber or possible contamination due to adsorbed organics. Detection of silicon, Si2s (99 eV), and phosphorous, P2p (130 eV) and P2s (190 eV), in the MPS-*co*-nAl and PAM-*co*-nAl powders, respectively, confirmed the presence of both monomers on the particles as these elements were not present in the neat powder but come from the silane and phosphoric acid moieties in the respective monomer. Because of background carbon present in the system, and possible carbon contamination in the neat nAl, the survey spectrum of CEA-*co*-nAl was not sufficient to confirm the addition of carbon (or oxygen); however, an increase in the O/Al and C/Al ratios (O/Al = 7.0, and C/Al = 3.4) from those in the neat nAl powder (O/Al = 5.0, and C/Al = 1.2), along with the TGA and FTIR data, confirms that the functionalization was successful.

Solvent Miscibility and Oxidation Resistance. The formation of bonds among the respective silane, carboxylic acid, and phosphoric acid portions of each ligand with the hydroxylated oxide surface orients the less polar acrylic portion of each ligand away from the particle surface, essentially forming a hydrophobic coating. The presence of this coating should enhance the miscibility of the functionalized particles in nonpolar media by masking the highly polar hydroxylated oxide surface. To determine whether the

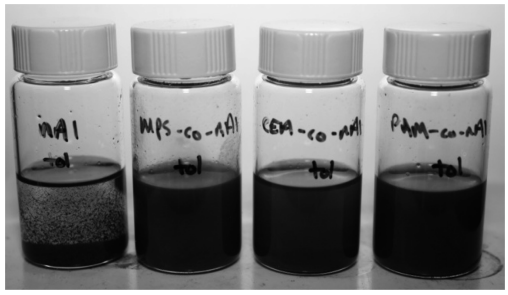

FIGURE 6. Picture of toluene suspensions prepared with nAl, MPS-*co*-nAl, CEA-*co*-nAl, and PAM-*co*-nAl (from left to right, respectively) after 1 min.

monomer coatings have had an impact on the stability and miscibility of nAl in common solvents, we prepared a series of suspensions designed to compare the stability of the functionalized powders to that of unfunctionalized nAl in common solvents and monomers. We prepared the suspensions by combining 0.030 g of the respective powder with 10 mL of solvent in a glass vial. The mixtures were then transferred to an ultrasonic bath for 60 s to suspend the particles. The solvents used for this study included water, toluene, ethanol, MMA, styrene, and lauryl methacrylate (LMA). MMA, styrene, and LMA were chosen as model monomers to represent mixtures that might be used to prepare a polymer nanocomposite from the functionalized nAl powders. Upon suspension, the vials were placed next to each other to compare their stability. This was done through careful observation of the time that was required for the particles to settle out of the suspensions. Images were acquired at various times during the settling process to document the visual appearance of the suspensions. In all of the suspensions studied, the particles did eventually settle out of the suspension, although the time required for complete settling varied widely between the suspensions, illustrating the differences in the chemical nature of coatings on the particles.

Suspensions prepared in toluene (Figure 6) were clearly more stable for the functionalized powders than for neat nAl, which began to settle immediately upon removal from the sonicator. Enhanced miscibility was also observed for suspensions prepared with the functionalized powders in both MMA and LMA, the exception being CEA-*co*-nAl which was only partially suspended in both momoners. A similar trend was also observed for ethanol, with CEA-*co*-nAl demonstrating partial miscibility and nAl, because of its polar oxide surface, being completely miscible. Fairly stable suspensions were also observed in styrene for all samples, including the neat nAl powder. A summary of the suspension stabilities is presented in Table 4. A collection of the images acquired for suspensions can be found in Figure S4 of the Supporting Information.

The most intriguing observations obtained from this study came from the suspensions that were prepared in water. Although our primary focus was to alter the surface chemistry of nAl to promote compatibility within organic systems such as polymers and solvents, to aid in the preparation of high-energy density nanocomposite materials, we also decided to study the effectiveness of these coatings in aqueous systems. Formulations of nAl and water (in the form of water or ice) have recently been demonstrated to be effective solid rocket propellants (6, 7). In general, nAl suspensions prepared in water are relatively unstable, as the particles oxidize over time, slowly consuming the metallic aluminum, yielding aluminum oxide and hydrogen as a gaseous byproduct. Our hypothesis was that the monomer coatings we have introduced might also provide a sufficient hydrophobic barrier that would limit diffusion of water to the particle surface, thereby extending the lifetime of the particles in aqueous media. To test this theory, we prepared suspensions of the functionalized powders in water and investigated their stability and resistance to oxidation in comparison to an aqueous suspension of neat nAl. As displayed in Figure 7a, stable suspensions were obtained for all of the powders in water with the exception, again, of CEA-*co*-nAl which was partially miscible and settled out of the suspension.

Table 3. FTIR Peak Positions and Assignments for Functionalized nAl Powders

sample	wavenumber (cm^{-1})	assignment
nAl	3330 (br)	O−H stretch
	900−750 (br)	Al−O stretch
MPS-*co*-nAl	2932	aliphatic C−H stretch
	1713	C═O in unsaturated ester
	1657	C═C stretch
	1191	C−O−C ester antisym stretch
CEA-*co*-nAl	3300 (br)	O−H stretch
	2978, 2940	aliphatic C−H stretch
	1719	C═O in unsaturated ester
	1577	COO^- antisym stretch
	1180	C−O−C ester antisym stretch
PAM-*co*-nAl	2986	aliphatic C−H stretch
	1724	C═O in unsaturated ester
	1641	C═C stretch
	1461	CH_2 scissor vibration
	954	P−O−C antisym stretch

The neat nAl powder was easily suspended in water, requiring minimal sonication; however, MPS-*co*-nAl significantly repelled the water and required significant sonication to be suspended. Even after sonication, MPS-*co*-nAl adhered to the sides of the glass vial. Only mild sonication was required to suspend PAM-*co*-nAl in water. After being prepared, all four suspensions were allowed to sit undisturbed. Although the particles eventually settled out from each of the suspensions during this period of time, oxidation occured in the nAl, CEA-*co*-nAl, and eventually MPS-*co*-nAl suspensions, which was easily observed through color changes in the powders (Figure 7b,c). Oxidation resulted in a transition from the original deep gray/black color to a lighter gray and finally to white. This was accompanied by the presence of bubbles in the solvent, presumably from the evolution of hydrogen gas. Noticeable oxidation of the neat nAl powder began after exposure to the water for 32 h, with complete oxidation occurring after 46 h. The functionalized particles demonstrated far better resistance to oxidation

Table 4. Summary of Particle Suspensions in Common Solvents

	toluene	ethanol	water	MMA	styrene	LMA
nAl	settled	miscible	miscible	settled	miscible	partially miscible
MPS-*co*-nAl	miscible	miscible	partially miscible	miscible	miscible	miscible
CEA-*co*-nAl	miscible	settled	partially miscible	partially miscible	miscible	settled
PAM-*co*-nAl	miscible	miscible	miscible	miscible	miscible	miscible

when compared to the neat powder. MPS-*co*-nAl and PAM-*co*-nAl both displayed significant resistance to oxidation, at room temperature, with the solutions retaining their original black color even after exposure to water for 144 h. As previously mentioned, CEA-*co*-nAl did eventually undergo oxidation during the 144 h time frame; however, this occurred more gradually than in the neat powder and was not complete even after 144 h, which can be seen by the gray aggregates of powder at the bottom of the vial in Figure 7b. Partial oxidation of MPS-*co*-nAl did eventually occur after exposure to water for ca. 350 h, yet the PAM-*co*-nAl suspension still showed no signs of oxidation, retaining its original dark gray/black color, after exposure at room temperature for more than 540 h (22.5 days). These results confirm trends observed in a similar study in which the stability of SAMs prepared with perfluorinated organosilanes, carboxylic acids, and phosphoric acids on bulk aluminum substrates in aqueous environments was observed (18).

In addition to the room-temperature aqueous oxidation study, we also investigated the integrity of the coatings when exposed to an elevated temperature of 75 °C to accelerate the rate of oxidation. It was not terribly surprising that trends

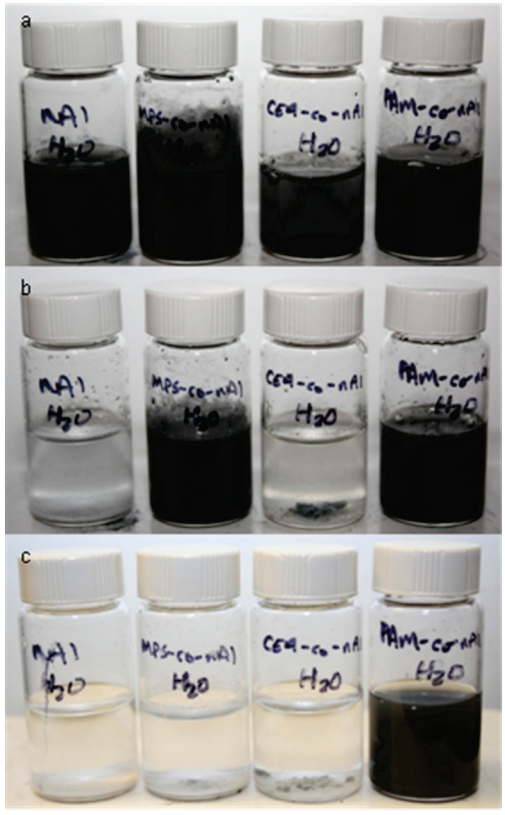

FIGURE 7. nAl, MPS-*co*-nAl, CEA-*co*-nAl, and PAM-*co*-nAl suspensions (from left to right, respectively) in water after (a) 1 min, (b) 144 h, and (c) 536 h at room temperature.

which paralleled the room-temperature study were also observed at elevated temperatures; however, an increase in the rate of oxidation was observed. Evolution of gas was observed in the MPS-*co*-nAl suspension after ca. 45 min; however, no visible color change was observed until 52 min, and oxidation was complete after 58 min. Gas evolution in the nAl suspension began at ca. 52 min, with noticeable oxidation occurring between 58 and 62 min. CEA-*co*-nAl began showing signs of oxidation after 66 min, with complete oxidation occurring after 74 min. Heat was removed from the suspensions after 3 h. The nAl, CEA-*co*-nAl, and MPS-*co*-nAl suspensions had all demonstrated significant oxidation, having turned mostly white in color. It is worth noting that the stability of the MPS coating was greatly affected by the elevated temperatures. Room-temperature oxidation of MPS-*co*-nAl did not occur until after 144 h, lasting far longer than that of nAl and CEA-*co*-nAl; however, at 75 °C the MPS-*co*-nAl suspension was the first sample to be oxidized, with oxidation occurring slightly before that of nAl. Surprisingly, the PAM-*co*-nAl suspension still displayed no visible signs of oxidation and retained its original color even after more than 2 hours at elevated temperatures. Images obtained from the accelerated oxidation study are presented in Figure S4 of the Supporting Information.

General Discussion. Consideration of the collective data presented above strongly suggests that functionalizaiton of nAl with acrylic monomers that contain reactive silane, carboxylic acid, and phosphoric acid moieties does significantly alter the chemistry of the nAl surface. Not only does the addition of the monomers to the particles' surface promote their dispersion and miscibility in common nonpolar solvents and in acrylic monomers, but we have also shown the monomeric coatings are also capable of influencing the oxidation resistance of the particles in aqueous environments. For all monomers studied, functionalization occurs through chemical attachment of the monomer to the oxide surface, either through reaction (condensation) with the hydroxyls present on the passivated oxide surface or with the oxidized aluminum atoms within the oxide. Through careful investigation of the FTIR and XPS data, we found that both MPS and PAM likely form covalent bonds to the oxide surface through reaction of the respective silane and phosphoric acid moieties with surface hydroxyls present on the oxide. The thermal stability of these coatings, under an inert atmosphere, also confirms that these coatings are likely anchored to the oxide through covalent bonds and are not merely physisorbed.

Interaction of CEA with the passivated oxided surface of nAl appears to occur through the ionic interaction of the carboxylate, COO^-, anion with oxidized aluminum (Al^{3+})

within the amporphous oxide. Additionally, it was clear from the TGA decomposition data for CEA-*co*-nAl that the monomer also undergoes thermally induced polymerization under the selected reaction conditions, which leads to the presence of polymer on the particle surface. This is not observed in the case of MPS or PAM.

It is clear from the miscibility studies that the monomeric coatings have an impact on the compatibility of nAl in organic solvents and polymeric systems, which was the primary motivation for performing this work. Improving the miscibility of nAl increases the likelihood of incorporating these powders in nanocomposites and future high-energy reactive materials. In addition to improving compatibility with organic systems, MPS and PAM monomer coatings also significantly reduce the degree of oxidation of nAl when exposed to aqueous environments. Though this was not the initial intention of this study, improving the oxidation resistance of nAl in aqueous environments could potentially be a critical enabler for emerging technologies such as nAl−water/ice-based propellants (6, 7) or beneficial in providing a controlled time release of hydrogen gas in nAl−water reactors (40, 41).

CONCLUSIONS

We report the successful grafting of three acrylic monomers, MPS, CEA, and PAM, to the amorphous oxide surface of nAl through reaction with the surface hydroxyls present at the particle surface or, in the case of CEA, interaction with Al^{3+} at the particle surface. Through calculation of their individual grafting densities, we found that MPS reacts to form a near monolayer on the particle surface while both CEA and PAM react to form multilayers. Additionally, we have shown that CEA also undergoes polymerization, even in the presence of an inhibitor, resulting a coating that consists of both monomer and polymer. Regardless of monomer, complete functionalization is achieved within 8 h. The functionalized particles demonstrate enhanced miscibility with nonpolar organic solvents and acrylic monomers in comparison to the unfunctionalized nAl powder. Additionally, the PAM and MPS coatings are effective at inhibiting oxidation of nAl in aqueous environments for extended periods of time at room temperature, while the PAM coating provides extended resistance to oxidation even at elevated temperatures. These findings could potentially have a strong impact on the processing of new high-energy density composite materials.

Acknowledgment. We thank Drs. C. E. Bunker, J. L. Jordan, C. M. Lindsay, K. A. S. Fernando, and W. K. Lewis for useful discussions and assistance with data collection. Additionally, we acknowledge Mr. W. A. Houston and Mr. J. M. Scott for technical support. Funding for this work was made available by Air Force Research Laboratory, Materials and Manufacturing Directorate, from the Nanoscience and Technology STT Initiative in Nanoenergetics. Their support is gratefully acknowledged. This research was performed while an author (C.A.C.) held a National Research Council Post-doctoral Research Associateship.

Supporting Information Available: TGA overlays for the decomposition of CEA monomer, CEA-*co*-nAl, and poly(CEA) and PAM monomer, PAM-*co*-nAl, and poly(PAM), XPS survey spectra acquired from functionalized and neat aluminum nanoparticles, digital images illustrating particle suspensions obtained in various solvents, and digital images demonstrating visible oxidation occurring during the heating of aqueous particle suspensions. This material is available free of charge via the Internet at http://pubs.acs.org.

REFERENCES AND NOTES

(1) Dreizin, E. L. *Prog. Energy Combust. Sci.* **2009**, *35*, 141–167.
(2) Levitas, V. I.; Asay, B. W.; Son, S. F.; Pantoya, M. *J. Appl. Phys.* **2007**, *101*, 083524.
(3) Sun, J.; Pantoya, M. L.; Simon, S. L. *Thermochim. Acta* **2006**, *444*, 117–127.
(4) Pantoya, M. L.; Granier, J. J. *Propellants, Explos., Pyrotech.* **2005**, *30*, 53–62.
(5) Brousseau, P.; Anderson, C. J. *Propellants, Explos., Pyrotech.* **2002**, *27*, 300–306.
(6) Ingenito, A.; Bruno, C. *J. Propul. Power* **2004**, *20*, 1056–1063.
(7) Risha, G. A.; Son, S. F.; Yetter, R. A.; Yang, V.; Tappan, B. C. *Proc. Combust. Inst.* **2007**, *31*, 2029–2036.
(8) Brege, J. J.; Hamilton, C. E.; Crouse, C. A.; Barron, A. R. *Nano Lett.* **2009**, *9*, 2239–2242.
(9) Jouet, R. J.; Warren, A. D.; Rosenburg, D. M.; Bellitto, V. J.; Park, K.; Zachariah, M. R. *Chem. Mater.* **2005**, *17*, 2987–2996.
(10) Gromov, A. A.; Forter-Barth, U.; Teipel, U. *Powder Technol.* **2006**, *164*, 111–115.
(11) Kwon, Y.-S.; Gromov, A. A.; Strokova, J. I. *Appl. Surf. Sci.* **2007**, *253*, 5558–5564.
(12) Foley, T. J.; Johnson, C. E.; Higa, K. T. *Chem. Mater.* **2005**, *17*, 4086–4091.
(13) Meziani, M. J.; Bunker, C. E.; Lu, F.; Li, H.; Wang, W.; Guliants, E. A.; Quinn, R. A.; Sun, Y.-P. *ACS Appl. Mater. Interfaces* **2009**, *1*, 703–709.
(14) Crouse, C. A.; Shin, E.; Murray, P. T.; Spowart, J. E. *Mater. Lett.* **2010**, *64*, 271–274.
(15) Balazs, A. C.; Emerick, T.; Russell, T. P. *Science* **2006**, *314*, 1107–1110.
(16) Wefers, K.; Mirsa, C. Oxides and Hydroxides of Aluminum. Alcoa Technical Paper No. 19; 1988.
(17) Oberg, K.; Persson, P.; Shchukarev, A.; Eliasson, B. *Thin Solid Films* **2001**, *397*, 102–108.
(18) DeRose, J. A.; Hoque, E.; Bhushan, B.; Mathieu, H. J. *Surf. Sci.* **2008**, *602*, 1360–1367.
(19) Lim, M. S.; Feng, K.; Chen, X.; Wu, N.; Raman, A.; Nightingale, J.; Gawalt, E. S.; Korakakis, D.; Hornak, L. A.; Tiperman, A. T. *Langmuir* **2007**, *23*, 2444–2452.
(20) Karaman, M. E.; Antelmi, D. A.; Pashley, R. M. *Colloids Surf., A* **2001**, *182*, 285–298.
(21) Taylor, C. E.; Schwartz, D. K. *Langmuir* **2003**, *19*, 2665–2672.
(22) Abel, M. L.; Watts, J. F.; Digby, R. P. *Int. J. Adhes. Adhes.* **1998**, *18*, 179–192.
(23) Kallury, K. M. R.; Cheung, M.; Ghaemmaghami, V.; Krull, U. J.; Thompson, M. *Colloids Surf.* **1992**, *63*, 1–9.
(24) Goldstein, C. S.; Weiss, K. D.; Drago, R. S. *J. Am. Chem. Soc.* **1987**, *109*, 758–761.
(25) Liakos, I. L.; McAlpine, E.; Chen, X.; Newman, R.; Alexander, M. *Appl. Surf. Sci.* **2008**, *255*, 3276–3282.
(26) Spori, D. M.; Venkataraman, N. V.; Tosatti, S. G. P.; Durmaz, F.; Spencer, N. D.; Zurcher, S. *Langmuir* **2007**, *23*, 8053–8060.
(27) Guo, Z.; Pereira, T.; Choi, O.; Wang, Y.; Hahn, H. T. *J. Mater. Chem.* **2006**, *16*, 2800–2808.
(28) Ash, B. J.; Rogers, D. F.; Weigand, C. J.; Schadler, L. S.; Siegel, R. W.; Benicewicz, B. C.; Apple, T. *Polym. Compos.* **2002**, *23*, 1014–1025.
(29) Liu, H.; Ye, H.; Zhang, Y. *Colloid Surf., A* **2008**, *315*, 1–6.
(30) Liu, H.; Ye, H.; Zhang, Y.; Tang, X. *Dyes Pigm.* **2008**, *79*, 236–241.
(31) Manufacturer reported average particle size (APS) and specific surface areas (SSA). (a) Alfa Aesar, aluminum powder (lot C11T058), 18 nm APS; SSA, not reported. (b) Nanostructured & Amorphous Materials, Inc., aluminum nanopowder (lot 0136-

010808), 18 nm APS; SSA, 40−60 m^2/g. (c) American Elements, aluminum metal nanopowder (lot 1031396379-818), 10−30 nm APS; SSA, 20−40 m^2/g.
(32) Wasserman, S. R.; Whitesides, G. M.; Tidswell, I. M.; Ocko, B. M.; Pershan, P. S.; Axe, J. D. *J. Am. Chem. Soc.* **1989**, *111*, 5852–5861.
(33) Adiga, S. P.; Zapol, P.; Curtis, L. A. *J. Phys. Chem. C* **2004**, *111*, 7422–7429.
(34) Hu, Y.-H.; Chen, C.-Y. *Polym. Degrad. Stab.* **2003**, *82*, 81–88.
(35) Holland, B. J.; Hay, J. N. *Polym. Degrad. Stab.* **2002**, *77*, 435–439.
(36) Fyfe, C. A.; McKinnon, M. S. *Macromolecules* **1986**, *19*, 1909–1912.
(37) Mauere, J. J.; Eustace, D. J.; Ratcliffe, C. T. *Macromolecules* **1987**, *20*, 196–202.
(38) Shek, C. H.; Lai, J. K. L.; Gu, T. S.; Lin, G. M. *Nanostruct. Mater.* **1997**, *8*, 605–610.
(39) Sah, A.; Castricum, H. L.; Bliek, A.; Blank, D. H. A.; ten Elshof, J. E. *J. Membr. Sci.* **2004**, *243*, 125–132.
(40) Martinez, S. S.; Sanchez, L. A.; Gallego, A. A. A.; Sebastian, P. J. *Int. J. Hyrdogen Energy* **2007**, *32*, 3159–3162.
(41) Soler, L.; Macanas, J.; Munoz, M.; Casado, J. *J. Power Sources* **2007**, *169*, 144–149.

AM100402Z